J. Phys. B: At. Mol. Opt. Phys. **29** (1996) 1397–1408. Printed in the UK

State-selective charge transfer in slow collisions of O^{3+} with H and H_2

J P M Beijers, R Hoekstra and R Morgenstern

KVI Atomic Physics, Rijksuniversiteit Groningen, Zernikelaan 25, 9747 AA Groningen, The Netherlands

Received 27 September 1995

Abstract. We have used photon emission spectroscopy to determine absolute, state-selective cross sections for single-electron capture by O^{3+} ions colliding on atomic and molecular hydrogen. The impact energy was varied between 45 and 752 eV amu^{-1}. For $O^{3+} + H$ collisions we find that the cross section for capture into the 2p3s state of O^{2+} strongly increases with impact energy up to an energy of ≈ 100 eV amu^{-1}. At higher impact energies the 2p3s cross section becomes comparable to the more or less constant 2p3p cross section. For the $O^{3+} + H_2$ system these state-selective cross sections both stay approximately constant over the entire energy range investigated. Our results will be compared with existing experimental and theoretical data.

1. Introduction

Single-electron capture (SEC) is the dominant process in collisions between multicharged ions and neutral particles in the low to intermediate energy regime ($E \leqslant$ a few keV amu^{-1}). The electron transfer occurs via quasi-resonant capture into excited states of the projectile ion with high probability [1]. Therefore SEC processes play a central role in the charge and energy balances of different types of plasma, e.g. fusion and astrophysical plasmas [2, 3]. Furthermore, observation of the line emission from the decaying product ions yields important information about several key plasma parameters. For these reasons much attention has been devoted in recent years to accurately determining the relevant cross sections both experimentally and theoretically [4].

The present paper describes an experimental study on SEC by B-like O^{3+} ions colliding on atomic and molecular hydrogen, with both reactants initially in their ground states:

$$O^{3+}(1s^2 2s^2 2p\ ^2P^o) + H/H_2 \rightarrow O^{2+}(1s^2 2s^2 2pnl) + H^+/H_2^+ . \qquad (1)$$

This reaction is particularly significant for several astrophysical plasmas where charge transfer is important, e.g. planetary nebulae [5, 6] and for the colder regions of tokamak plasmas. The observed O^{2+} emission lines resulting from reaction (1) can only be correctly interpreted when the relevant absolute, state-selective SEC cross sections are available. Thus several theoretical and experimental studies have been performed in order to determine the necessary data.

Dalgarno and collaborators have developed quantum-mechanical molecular orbital (MO) expansion methods to calculate state-selective SEC cross sections for reaction (1) [7–9]. They found that only the $1s^2 2s^2 2p3s$ and $1s^2 2s^2 2p3p$ configurations are populated in the O^{2+*} product ions for collision energies ranging from thermal up to 5000 eV amu^{-1}. The

0953-4075/96/071397+12$19.50

$1s^2 2s^2 2p3d$ configuration does not contribute significantly in this energy range. Gargaud also used the MO expansion method to calculate state-selective SEC cross sections for the O^{3+}+H collision [10]. She found that at collision energies above 20 eV amu^{-1} capture into the 3s state dominates, while for lower collision energies the 3p state is dominantly populated. In addition, Gargaud's calculation indicates that the 3p ^{1}S and ^{1}D cross sections can be neglected. The total SEC cross sections as calculated by both groups agree at the higher impact energies (above $\approx$300 eV amu^{-1}) but differ significantly for energies below 100 eV amu^{-1}.

A few groups have done experimental work on the $O^{3+} + H/H_2$ system. Church and Holzscheiter [11] measured the reaction rate constant for charge transfer in O^{3+}+H collisions at a temperature of 2.5×10^4 K in a Penning trap and found a value in good agreement with the calculation of Heil *et al*. Total SEC cross section measurements were performed by Phaneuf *et al* in the energy range between 42 and 4915 eV amu^{-1} via charge-state analysis [12]. This group succeeded a few years later in extrapolating the measurements to much lower collision energies (0.1 eV amu^{-1}!) by using merged-beam techniques [13]. The experimental total cross section data are generally better reproduced by Gargaud's calculation, although there remains a systematic discrepancy throughout the whole energy range. The first state-selective SEC cross sections for the $O^{3+} + H$ system were measured by Wilson *et al* using translational energy spectroscopy [14]. They found capture into the 3s state to be dominant for impact energies between 263 and 750 eV amu^{-1}. These results agree with their multichannel Landau–Zener (MCLZ) calculations which were used to put the relative cross sections on an absolute scale. However, the theoretical MCLZ total SEC cross sections are approximately a factor of two smaller than the ones determined experimentally by Phaneuf *et al* [12]. This was corroborated by an initial experiment of our group where we determined state-selective SEC cross sections for reaction (1) by using photon emission spectroscopy (PES) in the visible and VUV wavelength region at an impact energy of 1.5 keV amu^{-1} [15]. The advantage of the PES technique is the much higher resolution compared to translational energy spectroscopy, at the expense of a much lower detection efficiency. We found the 3s ^{3}P^o channel to be the dominant one, and the sum of the state-selective cross sections agreeing with the total SEC cross sections of Phaneuf *et al* [12].

The present paper reports an extension of our earlier work [15] to much lower impact energies ranging from 45 to 752 eV amu^{-1}, this time using only VUV PES. Our results will be discussed in the framework of the classical overbarrier model [16] and the multichannel Landau–Zener model [17], and compared with the experimental and theoretical results of other groups. We first give a brief description of the experimental apparatus and method of data analysis.

2. Experimental method

The apparatus used in the present investigation has already been described in detail in [18]. Here we give only a short description. The O^{3+} projectile ions are extracted from an ECR ion source at a fixed extraction voltage of 4 kV, transported to the collision chamber and, before being crossed with the target beam, decelerated with an electrostatic lens system to the desired collision energy. The collisions take place in a field-free region. After traversing the scattering centre the projectile ions are collected in a Faraday cup; the total accumulated charge is used for normalization purposes. Typical beam currents measured in the Faraday cup are between 0.3 and 0.4 μA. The primary-ion beam suffers from some metastable-ion contamination consisting of O^{3+} ions in the $1s^2 2s 2p^2$ ^{4}P configuration. Following [19] we estimate the metastable-ion fraction to be 0.12 ± 0.1, which agrees well with the value

of 0.16 found by Phaneuf *et al* [12]. In the data analysis only those emission lines are used to determine capture cross sections that are not contaminated with contributions from metastable parent ions.

In the scattering centre the projectile beam is crossed with a H/H_2 target beam produced with a Slevin-type radiofrequency (RF) source [20]. At each collision energy cross section measurements have been performed with pure H_2 and partly dissociated H/H_2 target beams. The dissociation degree of the mixed target beam was typically 70%. This important parameter is checked before and after each measurement by measuring the He II ($2p \rightarrow 1s$) line emission resulting from collisions between He^{2+} and H/H_2 at an impact energy of 5.33 keV amu^{-1}. These He^{2+} ions are easily extracted from the ECR ion source and transported through the beam line because the ion source is fed with a CO-He gas mixture and the magnetic rigidity of 5.33 keV amu^{-1} He^{2+} ions is the same as that for 0.75 keV amu^{-1} O^{3+} ions. The intensity of the He II ($2p \rightarrow 1s$) emission line is a sensitive indicator of the dissociation degree because the emission cross section for collisions on atomic hydrogen is almost a factor of three larger than on molecular hydrogen [21, 22]. In this way we found the target density stable within 1.5% and 3% for the pure H_2 and mixed H/H_2 target beams, respectively. The effective target pressure in the collision chamber is kept low enough to ensure single-collision conditions. Two pairs of Helmholtz coils surrounding the collision chamber reduce the magnetic field perpendicular to the ion beam to less than a few μT.

We use a 1 m grazing incidence VUV monochromator (10–80 nm) to observe the photon emission from the decaying product ions. A position sensitive detector enables simultaneous detection of lines within a range of about 20 nm. The wavelength resolution of the monochromator is approximately 0.6 nm. The relevant O III emission lines have wavelengths between 34 and 67 nm, which can be covered with two seperate measurements. The monochromator is placed under the magic angle of 54.7° with respect to the ion-beam axis and tilted by 45° in order to cancel all polarization-dependent effects. Lifetime corrections are not necessary since all the observed product states decay within view of the detection system. The wavelength-dependent sensitivity of the VUV monochromator has been determined absolutely with an uncertainty of 20% by means of various electron- and ion-impact processes with well known cross sections. Details of this procedure can be found in [23, 24]. A typical VUV spectrum in the 34–48 nm range resulting from $O^{3+} + H/H_2$ collisions at an impact energy of 100.7 eV amu^{-1} is shown in figure 1.

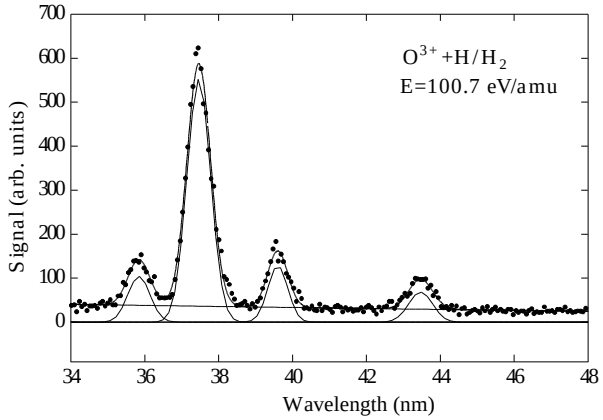

Figure 1. Typical VUV emission spectrum resulting from $O^{3+} + H/H_2$ collisions at an impact energy of 101 eV amu^{-1}.

3. Data analysis

3.1. O^{2+} VUV spectroscopy and cascade corrections

The O III spectrum in the 34–67 nm range results from the decay of the $1s^2 2s^2 2p$ 3s and 3p O^{2+} states of which a level diagram is shown in figure 2. The angular momentum coupling between the captured electron and the projectile core produces the singlet and triplet structure of the O III spectrum. Binding energies are taken from Kelly [25]. In agreement with the theoretical predictions we do not observe lines from $1s^2 2s^2 2p3d$ states in the VUV spectra. The wavelengths and branching ratios of the various VUV transitions are given in table 1 and have been obtained from [26, 27]. By inspection of the table it can be seen that the line emission from the 3p singlet states falls outside the present wavelength range. However, capture into the 3p ^{1}S and ^{1}D states can be neglected [10], so that the present experiment only misses the 3p ^{1}P state. As will be discussed below this cross section is also very small compared to the 3s singlet, triplet and 3p triplet ones.

Emission cross sections $\sigma_{\rm em}(nl \rightarrow mk)$ for the observed transitions are determined from the corresponding peak areas $S(\lambda)$ in the VUV spectra with the relation

$$\sigma_{\rm em}(nl \rightarrow mk) = \frac{4\pi}{\omega} \frac{q}{K(\lambda)Q} \frac{S(\lambda)}{NL} \tag{2}$$

where λ is the wavelength of the $nl \rightarrow mk$ transition, ω the solid angle of observation, q

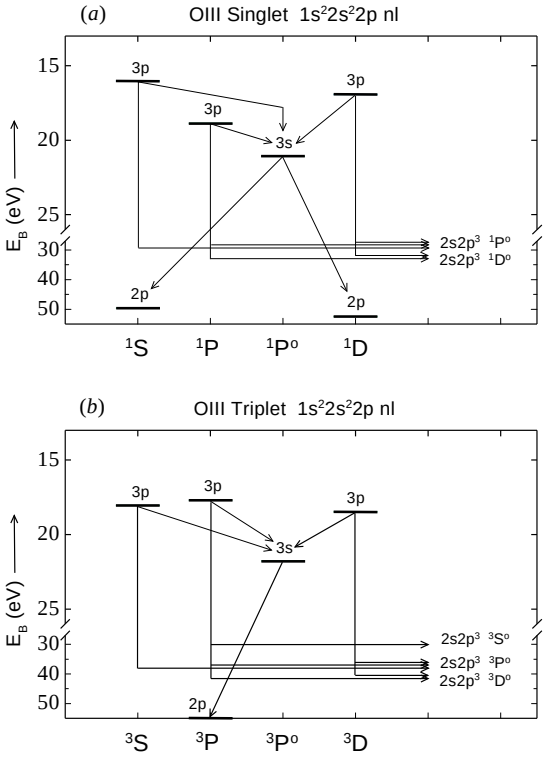

Figure 2. Energy level diagram of O^{2+}: (*a*) singlet system and (*b*) triplet system. Radiative transitions are denoted by straight lines.

Table 1. Wavelengths (in nm) of the relevant lines in the O III spectrum. The branching ratios of the various lines are indicated in parentheses.

Singlets		Upper state			
		$^1P^o$	^1S	^1P	^1D
Lower state		3s	3p	3p	3p
^1S	2p	43.5 (0.223)			
$^1P^o$	3s		245.5 (0.663)	559.2 (0.223)	298.4 (0.536)
	$2s2p^3$		99.2 (0.337)	129.5 (0.245)	107.4 (0.0656)
^1D	2p	39.6 (0.777)			
$^1D^o$	$2s2p^3$			98.1 (0.532)	84.9 (0.398)
Triplets		**Upper state**			
		$^3P^o$	^3S	^3P	^3D
Lower state		3s	3p	3p	3p
$^3S^o$	$2s2p^3$			99.3 (0.0036)	
^3P	2p	37.4 (1.00)			
$^3P^o$	3s		33.2 (0.498)	304.7 (0.732)	377.2 (0.649)
	$2s2p^3$		64.4 (0.502)	63.6 (0.156)	65.9 (0.310)
$^3D^o$	$2s2p^3$			55.4 (0.109)	57.4 (0.041)

the charge state of the projectile ions, Q the accumulated ion charge, $K(\lambda)$ the quantum yield of the detection system, N the effective target density and L the observation length. The accumulated ion charge Q in equation (2) is corrected for the fraction of metastables present in the primary-ion beam as discussed above.

State-selective cross sections for capture into the 3s and 3p states follow from the emission cross sections σ_{em} via the general relation

$$\sigma(nl) = \frac{\sigma_{\mathrm{em}}(nl \to mk)}{\beta_{nl,mk}} - \sum_{i>n} \sigma_{\mathrm{em}}(ik \to nl) \tag{3}$$

with $\beta_{nl,mk}$ the branching ratio for the $nl \to mk$ transition (table 1). The second term in equation (3) accounts for cascade contributions from higher populated states. This is only relevant for the 3s states as there are no states significantly populated above the 3p states.

3.2. Separation of the H and H_2 contributions

Before using equations (2) and (3) for determining emission and capture cross sections for the $O^{3+} + H$ system the H_2 contribution has to be subtracted from the spectra obtained with the partly dissociated H/H_2 target beam. In order to do this we have to determine the H and H_2 densities in the mixed target beam. As mentioned in section 2 this is done by observing the He II ($2p \to 1s$) line emission following $He^{2+} + H/H_2$ collisions. When the RF of the dissociator is turned off the He II ($2p \to 1s$) signal S^{off} is simply proportional to the effective H_2 density $N^{\mathrm{off}}(H_2)$ via

$$S^{\mathrm{off}} = CQN^{\mathrm{off}}(H_2)\sigma(H_2) \tag{4}$$

where $\sigma(H_2)$ is the cross section for capturing an electron into the $He^+(2p)$ state from a pure H_2 target and C a proportionality constant. With the RF turned on both the H and H_2 fractions of the mixed beam contribute to the signal S^{on}:

$$S^{\mathrm{on}} = CQ[N^{\mathrm{on}}(H)\sigma(H) + N^{\mathrm{on}}(H_2)\sigma(H_2)]\,. \tag{5}$$

Assuming a constant mass flux through the dissociator whether the RF is turned on or off and thermal equilibrium between both hydrogen components and the nozzle we find [28]

$$M_{H_2}\bar{v}^{off}(H_2)N^{off}(H_2) = M_{H_2}\bar{v}^{on}(H_2)N^{on}(H_2) + M_H\bar{v}^{on}(H)N^{on}(H) \tag{6}$$

with $\bar{v}(i)$ the average velocity and M_i the mass of component i, respectively. The atomic and molecular hydrogen densities $N^{on}(H)$ and $N^{on}(H_2)$ with RF turned on are then related to $N^{off}(H_2)$ via

$$N^{on}(H) = \sqrt{2}[N^{off}(H_2) - N^{on}(H_2)] \tag{7}$$

because $M_{H_2} = 2M_H$ and $\bar{v}(H) = \sqrt{2}\bar{v}(H_2)$ [28]. From equations (4), (5), (7) it follows that the ratio $N^{on}(H_2)/N^{off}(H_2)$ can be determined from the measured ratio S^{on}/S^{off} via

$$\frac{N^{on}(H_2)}{N^{off}(H_2)} = \frac{S^{on}/S^{off} - K}{1 - K} \tag{8}$$

with $K = \sqrt{2}\sigma(H)/\sigma(H_2) = 3.818$ at an impact energy of 5.33 keV amu^{-1} [21, 22]. The effective target density $N^{off}(H_2)$ in the pure H_2 beam is calibrated absolutely against a static H_2 target using a baratron. In this way we determine the effective H and H_2 densities in the mixed target beam before and after each measurement with the O^{3+} projectile beam. It is then straightforward to subtract the H_2 contribution from the signal S^{on} using the measured state-selective capture cross sections for the O^{3+} + H_2 system.

4. Experimental results

The state-selective SEC cross sections for O^{3+} ions colliding on H and H_2 as determined from the observed VUV spectra are given in tables 2 and 3. Also the result of our initial visible PES study at an impact energy of 1.5 keV amu^{-1} is tabulated in table 2 [15]. This study yielded for the 3p ^{1}P state: $\sigma(3p\ ^1P) = 0.8 \pm 0.2$ Å^2 and an upper limit of 0.5 Å^2 for the 3p ^{1}S,^{1}D states. We expect that these cross sections decrease with decreasing impact energy because of the very small splittings between the corresponding adiabatic potential energy curves [10]. In order to display the data we grouped the 3s and 3p cross sections, summed over both singlet and triplet states, together. These are shown in figures 3 and 5. Total capture cross sections are shown in figures 4 and 5. The uncertainty in the measurements comes from counting errors and target density fluctuations (statistical uncertainties) and from the sensitivity calibration of the VUV monochromator (systematic uncertainty). The errors

Table 2. State-selective [$\sigma(3l)$] and total [$\sigma(n = 3)$] SEC cross sections with corresponding statistical errors (one standard deviation) in units of 10^{-16} cm^2 for O^{3+} + H collisions.

E(eV amu^{-1})	σ(3s ^{1}P^o)	σ(3s ^{3}P^o)	σ(3p ^{3}S)	σ(3p ^{3}P)	σ(3p ^{3}D)	$\sigma(n = 3)$
1500[a]	3.20 ± 0.64	10.00 ± 2.00	1.10 ± 0.22	1.30 ± 0.26	5.00 ± 1.00	21.40 ± 2.36[b]
752	3.69 ± 0.37	8.72 ± 2.26	1.20 ± 0.23	3.16 ± 0.72	10.48 ± 2.41	27.25 ± 3.41
462	6.06 ± 0.46	12.08 ± 3.04	1.24 ± 0.24	2.79 ± 1.20	11.98 ± 3.24	34.15 ± 4.63
265	5.70 ± 0.47	9.03 ± 3.54	1.22 ± 0.36	2.67 ± 1.23	11.99 ± 3.98	30.61 ± 5.50
166	7.13 ± 0.82	14.91 ± 3.29	1.66 ± 0.29	4.00 ± 1.12	6.58 ± 2.58	34.28 ± 4.41
101	4.73 ± 0.76	3.78 ± 3.59	0.91 ± 0.27	2.18 ± 0.87	15.36 ± 3.13	26.96 ± 4.91
68	3.61 ± 0.60	0.28 ± 3.00	1.02 ± 0.27	3.27 ± 1.01	11.05 ± 2.85	19.22 ± 4.31
45	2.75 ± 0.52	0.00 ± 3.27	1.02 ± 0.30	3.12 ± 1.01	12.20 ± 3.38	19.08 ± 4.85

[a] See [15].
[b] Including $\sigma(3p\ ^1P) = 0.8 \pm 0.2$.

Table 3. State-selective [$\sigma(3l)$] and total [$\sigma(n = 3)$] SEC cross sections with corresponding statistical errors (one standard deviation) in units of 10^{-16} cm^2 for $O^{3+} + H_2$ collisions.

E(eV amu^{-1})	σ(3s ^{1}P^o)	σ(3s ^{3}P^o)	σ(3p ^{3}S)	σ(3p ^{3}P)	σ(3p ^{3}D)	$\sigma(n = 3)$
752	1.38 ± 0.10	2.51 ± 1.36	0.00 ± 0.17	1.57 ± 0.63	3.59 ± 1.50	9.04 ± 2.13
462	1.58 ± 0.18	1.89 ± 1.14	0.20 ± 0.14	3.19 ± 0.58	1.88 ± 1.22	8.74 ± 1.78
265	1.39 ± 0.18	1.90 ± 3.06	0.74 ± 0.43	5.63 ± 1.31	2.92 ± 3.49	12.58 ± 4.84
166	1.81 ± 0.26	5.44 ± 1.69	0.00 ± 0.18	3.33 ± 0.75	0.78 ± 1.55	11.36 ± 2.43
101	1.51 ± 0.25	4.00 ± 1.70	0.22 ± 0.18	3.17 ± 0.73	1.39 ± 1.33	10.29 ± 2.30
68	1.72 ± 0.33	5.92 ± 1.97	0.00 ± 0.13	4.67 ± 0.91	2.55 ± 1.35	14.86 ± 2.58
45	1.28 ± 0.24	3.64 ± 1.58	0.00 ± 0.12	3.38 ± 0.69	1.12 ± 1.20	9.41 ± 2.12

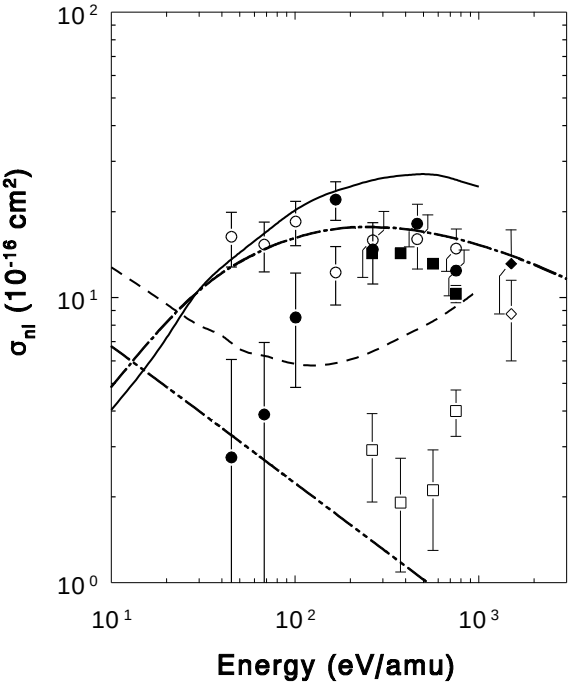

Figure 3. State-selective cross sections for capture into the $1s^2 2s^2 2p3l$ state of O^{2+} following $O^{3+} + H$ collisions. Experiment: (ϟ) 3s, (○) 3p, present; (♦) 3s, (◊) 3p, Hoekstra *et al* [15]; (■) 3s, (□) 3p, Wilson *et al* [14]. Theory: (— · —) 3s, (— · · —) 3p, present MCLZ; (——) 3s, (– – –) 3p, Gargaud [10].

given with the data correspond with one standard deviation of the statistical uncertainty; the additional systematic uncertainty of 20% is not included. A more detailed error discussion relevant to the present experiment can be found in [18].

5. Discussion

Before comparing the present results in detail with those of other groups it is instructive to make a comparison with the predictions of the (semi)classical overbarrier and Landau–Zener models. It is well known that both models describe the gross features, i.e. crossing radii and

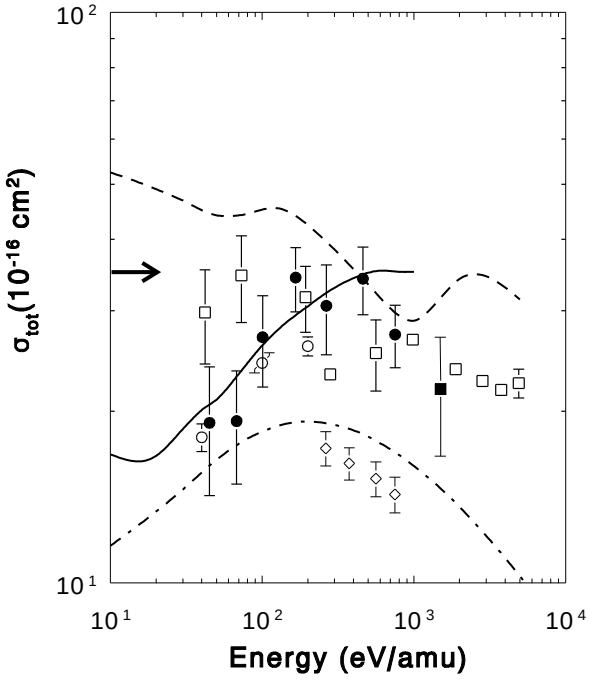

Figure 4. Total cross sections for capture into the $n = 3$ state of O^{2+} following $O^{3+} + H$ collisions. Experiment: (ϟ), present; (■), Hoekstra *et al* [15]; (○), Havener *et al* [13]; (□), Phaneuf *et al* [12]; (◊), Wilson *et al* [14]. Theory: (— · —), present MCLZ; (——), Gargaud [10]; (– – –), Bienstock *et al* [8].

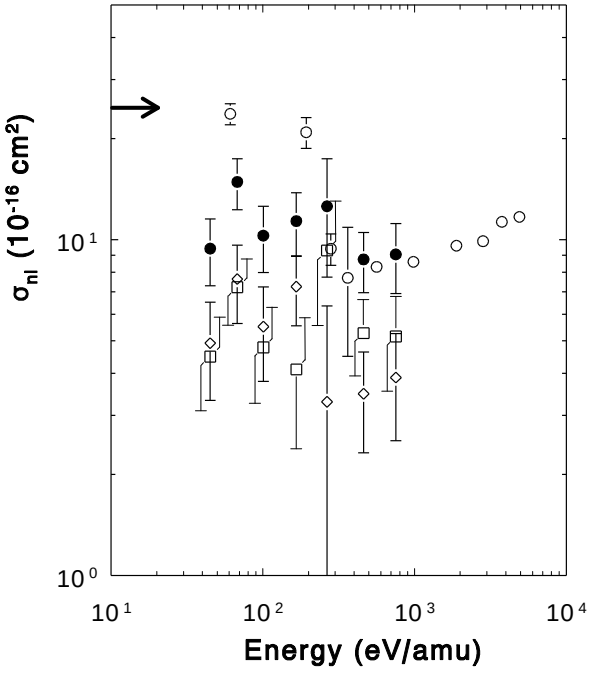

Figure 5. State-selective and total cross sections for capture into the $1s^22s^22p3l$ state of O^{2+} following $O^{3+} + H_2$ collisions. Experiment: (◊) 3s, (□) 3p, (ϟ) total, present; (○) total, Phaneuf *et al* [12].

total capture cross sections, of the charge transfer process fairly well [1]. According to the classical overbarrier model the charge transfer takes place when the distance between the collision partners has decreased to the point where the Coulombic barrier, which separates

the potential wells of projectile and target nuclei, drops below the binding energy of the active electron. This happens at a radius R_{CB} which only depends on the charge q of the projectile ion and the ionization energy I_t of the target via

$$R_{CB} = \frac{2q^{1/2} + 1}{I_t} . \tag{9}$$

The electron is transferred resonantly from target to projectile, so that its asymptotic binding energy I_q at the projectile ion is given by [16]

$$I_q = I_t + \frac{q - 1}{R_{CB}} . \tag{10}$$

The total SEC cross section is assumed to be proportional to the geometrical cross section

$$\sigma_t = A\pi R_{CB}^2 \tag{11}$$

and independent of the impact energy. The proportionality constant $A = 0.5$ yields good overall agreement with existing data for collisions with atomic and molecular hydrogen [29]. The estimates for the total SEC cross section according to equation (11) are denoted by horizontal arrows in the left margins of figures 4 and 5. As can be seen the agreement for the $O^{3+} + H$ system is excellent, while the classical prediction for the $O^{3+} + H_2$ system overestimates the experimental values.

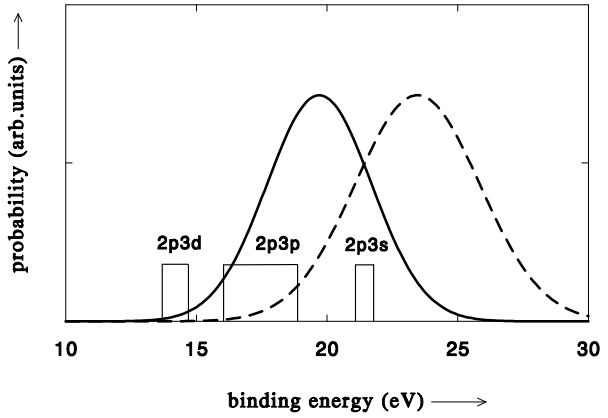

Figure 6. Reaction windows for electron capture in collisions of 752 eV amu^{-1} O^{3+} with atomic (——) and molecular (– – –) hydrogen.

The classical overbarrier model allows more qualitative insight into the total and state-selective capture cross sections by comparing the asymptotic binding energy I_q (equation (10)) of the captured electron with the binding energies of the various $3l$ states of the O^{2+} product ion. Actually, because of the finite time available for the charge transfer the binding energy I_q acquires an uncertainty. This is shown in figure 6 by the Gaussian reaction windows centred around I_q and with a width ΔE proportional to the square root of the impact velocity v [16]. Both reaction windows in figure 6 are calculated for an impact energy of 752 eV amu^{-1}. It is immediately evident that the $3l$ states are much more resonant with respect to the H window than with the H_2 window. One can therefore expect that the classical prediction of the total capture cross section will agree better with experiment for the $O^{3+} + H$ system than for the $O^{3+} + H_2$ system. Figures 4 and 5 show that this expectation is indeed justified. Furthermore, the off-resonant position of the 3d states relative to both reaction windows explains the fact that their capture cross sections can be neglected with respect to the 3s and 3p cross sections. The reaction window concept

is therefore a convenient tool for understanding qualitatively the magnitudes of total and state-selective capture cross sections.

In addition, we have calculated state-selective and total SEC cross sections for the O^{3+}+H system with the multichannel Landau–Zener model. The general application of this model to SEC transitions in collisions between multiply-charged ions and neutral atoms is reviewed in [1]. Our implementation of the model uses Olson–Salop–Taulbjerg transition matrix elements [17]. We have performed separate MCLZ calculations for the four singlet and for the four triplet channels enumerated in table 1. The 3s and 3p cross sections are then calculated by averaging over the relevant channels with a weighting factor of $\frac{1}{4}$ for the singlet and $\frac{3}{4}$ for the triplet channels, respectively. Our MCLZ results are shown in figures 3 and 4. As can be seen, the calculated 3s cross sections reproduce the experimental ones for impact energies down to approximately 100 eV amu^{-1}, but decrease much more slowly for energies below this value than the experimental cross sections do. On the other hand, the calculated 3p cross sections decrease monotonically with increasing impact energy and underestimate the more or less constant experimental 3p cross sections. The reason for this discrepancy is probably attributable to the neglect of rotational coupling in the MCLZ model, which tends to become more important with increasing impact energies. We noticed the same shortcoming of the MCLZ model in our earlier study of SEC in collisions between He-like ions and He [30]. The total MCLZ capture cross sections are shown in figure 4 and underestimate the experimental data points for energies above 80 eV amu^{-1}. The reason for this is that the MCLZ theory fails to reproduce the 3p cross sections as discussed above.

Figure 3 also shows the state-selective results of the MO calculations by Gargaud [10]. The MO 3s cross sections show the same energy dependence as the MCLZ cross sections, but they lie above the experimental 3s cross sections over almost the entire energy range. The MO 3p cross sections decrease with increasing impact energy until approximately 100 eV amu^{-1} and increase again for higher impact energies. Although the MO 3p cross sections lie below the experimental data points they are a big improvement compared to the MCLZ theory. This shows the increasingly important role of rotational coupling at higher impact energies which is taken into account in the MO calculation. Furthermore, Gargaud's MO calculation indicates that the 3p ^{1}S and ^{1}D cross sections can be neglected compared to the total capture cross section. The reason for this is the completely diabatic behaviour of the system because of the very small splittings of the relevant potential energy curves. The upper limit of 0.5 Å^2 for these cross sections as determined in our visible PES study at an impact energy of 1.5 keV amu^{-1} is consistent with these predictions [15]. Total MO cross sections are shown in figure 4 together with the MO calculations of Bienstock *et al* [8]. The calculation of Gargaud nicely reproduces our experimental data. On the other hand, the calculation of Bienstock *et al* significantly overestimates the total SEC cross section particularly for smaller impact energies.

We will now compare our experimental data with other published experimental results. The only other state-selective data for the O^{3+} + H system are those of Wilson *et al*, also shown in figure 3 [14]. They used translational energy spectroscopy which, however, did not resolve the fine structure of the 3s and 3p multiplets. Wilson *et al* also performed MCLZ calculations which were used to put their relative cross sections on an absolute scale. Their MCLZ calculations yield slightly lower cross sections than our calculations, probably because of small differences between the potential energy curves used. The normalization procedure applied by Wilson *et al* prohibits comparison of the absolute numbers but, as figure 3 shows, even the relative cross sections differ from our data. The reason for this discrepancy is unclear. The total SEC cross sections obtained with several different techniques are collected in figure 4. As already discussed above our data do not include the contributions

of the 3p singlet states which, however, are expected to be very small. Phaneuf *et al* used a pulsed-laser ion source and time-of-flight technique for impact energies between 42 and 4915 eV amu^{-1} [12]. Havener *et al* extended these measurements to impact energies as low as 0.1 eV amu^{-1} with a merged-beam apparatus [13]. The agreement between both data sets of the Oak Ridge group and our measurements is good, apart from the two lowest data points of Phaneuf *et al*. Also the total SEC cross sections of Wilson *et al* are shown [14].

Finally, for the $O^{3+} + H_2$ system we can only compare our total SEC cross sections with those of Phaneuf *et al* [12]. Figure 5 shows that the agreement between both data sets is good, except at the lowest energies investigated where our data are below those of Phaneuf *et al*. Our state-selective data show that the 3s and 3p cross sections are more or less comparable in magnitude. The large statistical scatter in the data does not allow us to make more definitive statements.

6. Conclusions

In this paper we have studied single-electron capture in collisions between O^{3+} projectile ions and atomic and molecular hydrogen. Photon emission spectroscopy has been used to determine state-selective and total single-electron capture cross sections for the dominantly populated $1s^2 2s^2 2p3l$ states in the impact energy range between 45 and 752 eV amu^{-1}. The observed spectra do not allow us to determine capture cross sections for the 3p singlet states which, however, are expected to be very small. Our experimental results are in good agreement with the total cross section measurements of Phaneuf *et al* [12] and Havener *et al* [13], but differ from the state-selective cross section measurements of Wilson *et al* [14] for the $O^{3+} + H$ system.

Furthermore, we have performed classical overbarrier and Landau–Zener model calculations for the $O^{3+} + H$ collision system. These show that the classical overbarrier model yields a fairly good estimate of the total SEC cross section. In addition, the classical model gives some qualitative insight into the state-selectivity of the capture process by using the reaction window concept. The Landau–Zener model enables a more detailed comparison. This model reproduces the 3s cross sections above impact energies of approximately 100 eV amu^{-1}, but fails to reproduce the more or less constant 3p cross sections. This discrepancy is attributed to the neglect of rotational coupling in the Landau–Zener model. Finally, we have compared the present data with the more sophisticated MO calculations of Gargaud [10] and Bienstock *et al* [8]. Gargaud's calculation reproduces the total SEC cross section very well, although it overestimates the 3s cross section and underestimates the 3p cross section but exhibits the correct energy dependence of both cross sections. The calculation of Bienstock *et al* overestimates the total SEC cross section particularly for the smaller impact energies.

Collisions between intermediate-charge state ions of C and O with H, H_2 and He at very low impact energies are important for understanding interactions of the edge plasma such as occur in the divertor region of large tokamaks. We will add in the near future a high resolution grazing incidence VUV spectrometer to our recently completed collision chamber incorporating an RF octopole for ion guiding [31]. In this way we will be able to extend our study of charge transfer in the above-mentioned collision systems to lower impact energies (< 1 eV amu^{-1}) and with a higher resolution in the photon channel.

Acknowledgments

We wish to thank J Eilander and J Sijbring for their excellent technical support. This work is part of the research program of the 'Stichting voor Fundamenteel Onderzoek der Materie' (FOM) with financial support from the 'Stichting voor Nederlands Wetenschappelijk Onderzoek' (NWO). It also receives support from EURATOM via an article 14 contract between JET Joint Undertaking and KVI.

References

[1] Janev R K and Winter H 1985 *Phys. Rep.* **117** 265
[2] Summers H P *et al* 1991 *Z. Phys.* D **21** S17
[3] Fawcett B C 1991 *Z. Phys.* D **21** S1
[4] Fritsch W and Lin C D 1991 *Phys. Rep.* **202** 1
[5] Dalgarno A and Sternberg A 1982 *Astrophys. J. Lett.* **287** L87
[6] Clegg R E S and Walsh J R 1985 *Mon. Not. R. Astron. Soc.* **215** 323
[7] Heil T G, Butler S E and Dalgarno A 1983 *Phys. Rev.* A **27** 2365
[8] Bienstock S, Heil T G and Dalgarno A 1983 *Phys. Rev.* A **27** 2741
[9] Roueff E and Dalgarno A 1988 *Phys. Rev.* A **38** 93
[10] Gargaud M 1987 *Doctoral Thesis* L'Université de Bordeau I
[11] Church D A and Holzscheiter H M 1982 *Phys. Rev. Lett.* **49** 643
[12] Phaneuf R A, Alvarez I, Meyer F W and Crandall D H 1982 *Phys. Rev.* A **26** 1892
[13] Havener C C, Meyer F W and Phaneuf R A 1992 *Electronic and Atomic Collisions* ed W R MacGillivray, I E McCarthy and M C Standage (Bristol: IOP Publishing)
[14] Wilson S M, McCullough R W and Gilbody H B 1988 *J. Phys. B: At. Mol. Opt. Phys.* **21** 1027
[15] Hoekstra R, Boorsma K, de Heer F J and Morgenstern R 1989 *J. Physique Colloq.* **50** 349
[16] Niehaus A 1986 *J. Phys. B: At. Mol. Phys.* **19** 2925
[17] Taulbjerg K 1986 *J. Phys. B: At. Mol. Phys.* **19** L367
[18] Hoekstra R, Beijers J P M, Schlatmann A R, Morgenstern R and de Heer F J 1990 *Phys. Rev.* A **41** 4800
[19] Brazuk A, Dijkkamp D, Drentje A G, de Heer F J and Winter H 1984 *J. Phys. B: At. Mol. Phys.* **17** 2489
[20] Ćirić D, Dijkkamp D, Vlieg E and de Heer F J 1985 *J. Phys. B: At. Mol. Phys.* **18** 4745
[21] Hoekstra R, de Heer F J and Morgenstern R 1991 *J. Phys. B: At. Mol. Opt. Phys.* **24** 4025
[22] Hoekstra R, Folkerts H O, Beijers J P M, Morgenstern R and de Heer F J 1994 *J. Phys. B: At. Mol. Opt. Phys.* **27** 2021
[23] Kadota K, Dijkkamp D, van der Woude R L, de Boer A, Pan G Y and de Heer F J 1982 *J. Phys. B: At. Mol. Phys.* **15** 3275
[24] Dijkkamp D, Čirič D, Vlieg E, de Boer A and de Heer F J 1985 *J. Phys. B: At. Mol. Phys.* **18** 4763
[25] Kelly R L 1987 *J. Phys. Chem. Data* **16** Suppl. 1
[26] Striganov A R and Sventitskii N S 1968 *Tables of Spectral Lines of Neutral and Ionized Atoms* (New York: Plenum)
[27] Behringer K, Denne B, Forrest M, Stamp M and Summers H P 1989 *Internal Report* P(89)05, JET Joint Undertaking
[28] Walker J D and St John R M 1973 *J. Chem. Phys.* **61** 2394
[29] Ryufuku H, Sasaki K and Watanabe T 1980 *Phys. Rev.* A **21** 745
[30] Beijers J P M, Hoekstra R and Morgenstern R 1994 *Phys. Rev.* A **49** 363
[31] Bliek F W, Hoekstra R and Morgenstern R 1995 *Hyperfine Interactions* submitted